Journal of Atmospheric and Terrestrial Physics, Vol. 44, No. 12, pp. 1113–1122, 1982.
Printed in Great Britain.

0021–9169/82/121113–10 $03.00/0

VLF/ELF radiation from the ionospheric dynamo current system modulated by powerful HF signals

A. J. FERRARO, H. S. LEE, R. ALLSHOUSE, K. CARROLL

Ionosphere Research Laboratory, Electrical Engineering Department, Pennsylvania State University, University Park, PA 16802, U.S.A.

A. A. TOMKO

IIT Research Institute, Annapolis, MD 21401, U.S.A.

F. J. KELLY

Space Science Division, Naval Research Laboratory, Washington, DC, 20375, U.S.A.

and

R. G. JOINER

Electronics Division, Office of Naval Research, Arlington, VA 22217, U.S.A.

Abstract—This paper presents results of several campaigns at the Arecibo Observatory using the new HF high power 'heater' facility. The specific measurement pertains to detecting VLF/ELF radiation from the ionospheric dynamo current system that has been periodically modified by pulsing the HF high power transmitter at VLF or ELF. Because of the nonlinear relationship between ionospheric conductivities and electron temperature, the high power HF source can produce modification of the ionospheric conductivities and consequently of the dynamo current system. That this effect indeed does occur is verified by detecting the VLF/ELF radiation from this current source. Most of the data presented in this paper are concerned with measurements made at ground level beneath the modified current region. Limited data are presented for ELF signals received in Pennsylvania, U.S.A., over a long path from the HF 'heater' facility at Tromsø, Norway.

1. INTRODUCTION

An elementary description of the generation of ELF and VLF radiations by HF modification of the ionospheric current system is first presented. This phenomenon involves the irradiation of the ionospheric plasma by a strong HF wave which is modulated at some frequency, Ω. The periodic plasma heating that results from this wave is responsible for the emission of radio waves at a frequency Ω from the ionospheric current system; hence this effect is commonly referred to as nonlinear demodulation or ionospheric detection.

The basic physics of the nonlinear demodulation effect is illustrated in Figs 1 and 2. The electrons, within the area of plasma irradiated by the HF beam, experience periodic heating at the HF modulation frequency. Since the ionospheric conductivity is electron temperature dependent, the conductivity undergoes a similar periodic variation. Natural ionospheric currents (e.g. dynamo, polar electrojet, and equatorial electrojet) which pass through the heated region are modulated by the conductivity changes. Under ambient conditions the density of the ionospheric current is given by

$$\mathbf{J}_0 = \sigma_0 \mathbf{E}_G, \tag{1}$$

where $\mathbf{E}_G$ is the strength of the geoelectric field which drives the currents and $\sigma_0 = \sigma(T_a)$ is the ambient conductivity tensor. Within the heated region, the current density is

$$\mathbf{J} = \sigma(T_e)\mathbf{E}_G = \mathbf{J}_0 + \Delta\sigma(T_e)\mathbf{E}_G, \tag{2}$$

where

$$\Delta\sigma(T_e) = \sigma(T_e) - \sigma_0. \tag{3}$$

Thus, HF modulation of the ionospheric conductivity gives rise to a periodic current at the modulation frequency, Ω, of density

$$\mathbf{J}_\Omega = \Delta\sigma(T_e)\mathbf{E}_G. \tag{4}$$

This current is a source of Ω-frequency radiation, radiated by a novel type of antenna system.

Nonlinear demodulation phenomena of the type described above were observed during the Soviet heating experiments at Gorkii (GETMANTSEV *et al.*, 1974). During these experiments the polar currents

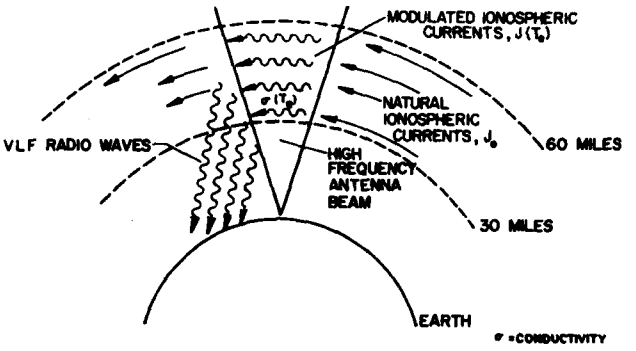

Fig. 1. Geometry of the nonlinear demodulation experiment.

were modulated at frequencies from 1 to 7 kHz using a 5.75 MHz carrier with an effective radiated power of 15 MW. Signals were regularly observed during the daytime at 2.5 and 4 kHz but not at 1 or 7 kHz. The field strength at 2.5 kHz varied from 2×10^{-2} to 25×10^{-2} μV m^{-1}. A distinct diurnal variation of the signal was reported, with the intensity reaching a maximum at noon and being generally unobservable at nighttime. Subsequent measurements by BUDILIN *et al.* (1977) have shown that the average height of the region of generation of the nonlinear current, $\mathbf{J}_\Omega$, is about 75 km.

The above results were for magnetically quiet conditions. GETMANTSEV *et al.* (1974) also report that measurements performed under magnetically disturbed conditions show that the VLF field is highly variable during these conditions and that the signal strength sometimes greatly exceeds the intensity of signals received during magnetically quiet conditions. Nighttime measurements by KAPUSTIN *et al.* (1977) during geomagnetic disturbances show that the observed VLF signal strength is well correlated with the strength and position of auroral currents as detected by groundbased magnetometers. The VLF signals were absent during magnetically quiet nighttime conditions.

Recently, TURUNEN *et al.* (1980) and STUBBE (1980) have reported the observation of VLF/ELF signals due to nonlinear demodulation of MF and HF waves during geomagnetic disturbances in northern Scandinavia. STUBBE (1980) observed a maximum signal strength near 2.5 kHz.

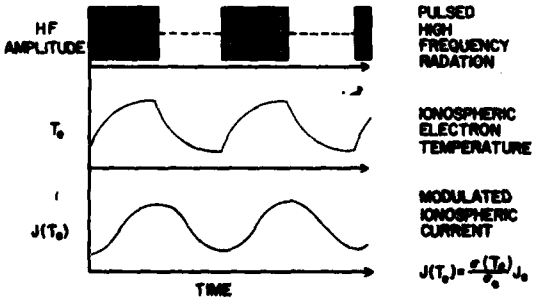

Fig. 2. Diagram showing ELF/VLF modulated ionospheric current by HF heating.

2. THEORY OF VLF/ELF RADIATION

2.1. *Heating theory*

If one neglects the effects of electron thermal conductivity and plasma transport, the electron energy balance equation can be written simply as

$$\tfrac{3}{2} n_e K_B \frac{\partial T_e}{\partial t} = P_e - \sum_j \left(\frac{dU}{dt}\right)_{e,j} \qquad (5)$$

where T_e is the electron temperature, n_e the electron density, K_B the Boltzmann's constant, P_e the rate of electron thermal energy production due to HF heating, and $(dU/dt)_{e,j}$ is the rate of electron thermal energy loss due to the jth collisional process between electrons and neutral particles. It is assumed that the electron and neutral particle energy distributions are Maxwellian and characterized by temperatures T_e and T_n, respectively, with $T_e = T_n$ prior to the introduction of HF heating.

When a region of the ionosphere is illuminated by an HF source radiating at frequency f, the local power density S at height h is given by

$$S(h) = S_0 \left(\frac{h_0}{h}\right)^2 \exp\left[-2k \int_{h_0}^{h} \chi(h')\, dh'\right], \qquad (6)$$

where $S_0 = P_T G/4\pi h_0^2$, the power density at some reference height h_0 below the base of the ionosphere, and P_T is the transmitter power (rectangular heating pulse assumed), G the antenna gain over isotropic radiation, k the free space propagation constant, and

$\chi(h')$ the absorption index at height h'. The HF source is assumed to be radiating vertically in a narrow beam over which the antenna gain is essentially constant.

Differentiating equation (6) with respect to height, one obtains

$$\frac{\partial S}{\partial h} = -\frac{2}{h}S - 2k\chi S. \tag{7}$$

The first term on the right accounts for the decrease in power density as the HF beam spreads with increasing height, while the second term represents the power dissipation per unit volume as a result of absorption by electrons. One can, therefore, write

$$P_e = 2k\chi S. \tag{8}$$

As a heating pulse propagates through the ionosphere, energy is absorbed from it and converted to electron heating as dictated by equation (8). Electron heating modifies the absorbing properties in the region of propagation, since χ is a function of T_e through its dependence on the electron-neutral collision frequency $\nu(T_e)$. Thus the heating pulse causes additional absorption on itself.

Electron heating results for a strong field have been given in great detail by TOMKO (1981). These results were obtained numerically from equations (5), (6) and (8); a few salient features can be stated here. After sustained CW heating, electron temperatures can be increased by about 700 K at 70 km during a daytime *D*-region, with an effective radiated power (ERP) of 100 MW using a 5.0 MHz, x-mode HF signal. Under pulsed conditions, at 70 km due to a 250 μs, 5 MHz x-mode signal, the electron temperature reaches a steady state in less than 250 μs and the plasma cools somewhat faster than it heats up for 100 MW ERP. The available power density at 70 km remains constant with time. This is not the case in the upper *D*-region (90 km); here the power density drops abruptly, from its initial value, to a steady-state value on a time scale of about 500 μs. This effect is due to self-absorption. The electron temperature at 90 km, on the other hand, responds much more slowly than the power density, requiring about 3.5 ms to reach a steady-state level. Self-absorption severely limits the available heating power in the upper *D*-region.

2.2. *Ionospheric conductivities*

The periodic temperature variations due to pulsing the HF heater at a VLF/ELF rate can alter the ionospheric conductivities in two ways. On short-time scales, the collision frequency is modified, while on longer time scales (i.e. $> 10^{-2}$ s) the electron density will be modified. The manner in which σ depends upon ν_{en} and n_e, the electron-neutral collision frequency and the electron density, is given by

$$\sigma_P(T_e) = n_e(T_e)\frac{e^2}{m_e}\frac{\nu_{en}(T_e)}{\omega_G^2 + \nu_{en}^2(T_e)}, \tag{9a}$$

$$\sigma_H(T_e) = n_e(T_e)\frac{e^2}{m_e}\frac{\omega_G}{\omega_G^2 + \nu_{en}^2(T_e)}, \tag{9b}$$

$$\sigma_L(T_e) = n_e(T_e)\frac{e^2}{m_e}\frac{1}{\nu_{en}(T_e)}, \tag{9c}$$

where σ_P, σ_H, and σ_L are the Pedersen (or Transverse), Hall, and Longitudinal conductivities, respectively. In this work it is assumed that the heating periods are short enough that electron density modifications do not occur.

The relationships between electron-neutral collision frequency (s^{-1}) and electron temperature (K) as given by BANKS and KOCKARTS (1973) are

$$\nu_{N_2} = 9.32 \times 10^{-12} n_{N_2} (1 - 3.44 \times 10^{-5} T_e) T_e, \tag{10a}$$

$$\nu_{O_2} = 1.21 \times 10^{-10} n_{O_2} (1 + 2.15 \times 10^{-2} T_e^{1/2}) T_e^{1/2}, \tag{10b}$$

$$\nu_O = 5.49 \times 10^{-10} n_O T_e^{1/2}, \tag{10c}$$

where n_{N_2}, n_{O_2} and n_O are the density of N_2, O_2 and O, respectively (cm^{-3}).

Because of the limited vertical extent of the ionospheric *E*-region, charges accumulate at the boundaries of the conducting layers; thus the resulting vertical component of dynamo current will cease to flow. The current then is horizontally directed. Under these conditions the conductivity tensor can be reduced from a 3×3 tensor to a 2×2 tensor. Using x and y coordinates for magnetic south and east, the layer conductivity can be expressed, following RISHBETH and GARRIOTT (1969), as

$$\sigma' = \begin{bmatrix} \sigma_{xx} & \sigma_{xy} \\ -\sigma_{xy} & \sigma_{yy} \end{bmatrix}, \tag{11}$$

where

$$\sigma_{xx} = \frac{\sigma_L \sigma_P}{\sigma_L \sin^2 I + \sigma_P \cos^2 I}, \tag{12a}$$

$$\sigma_{xy} = \frac{\sigma_L \sigma_H \sin I}{\sigma_L \sin^2 I + \sigma_P \cos^2 I}, \tag{12b}$$

and

$$\sigma_{yy} = \frac{\sigma_H^2 \cos^2 I}{\sigma_L \sin^2 I + \sigma_P \cos^2 I} + \sigma_P, \tag{12c}$$

with I being the magnetic dip angle.

Thus periodic temperature variations will cause periodic variations in σ_{xx}, σ_{xy}, and σ_{yy}, in turn modulating the horizontal current system.

2.3. *VLF/ELF radiation concept*

Estimates of the radiated fields observed at ground level directly underneath the modulated currents follow rather directly from classical antenna theory. The spatial volume of modified current fills the region of plasma that is intersected by the main beam of the HF heater antenna pattern. This is approximated as shown in Fig. 3 by an 'inverted' pyramid. Heights H_B and H_T define the vertical extent of the modified currents which in turn depend upon the values of σ_{xx}, σ_{yy}, and σ_{xy} under ionospheric and heating parameters. The region from H_B to H_T is decomposed into current sheets each having a thickness of 1.0 km. The approximate E and H fields calculated for ground level can be easily expressed (RICHARDSON, 1982) and summed over all current sheets between H_B and H_T. The radiation computer code thus will allow numerical evaluation of these fields once the modified currents as a function of altitude are computed.

2.4. *Computational methods*

Sections (2.1)–(2.3) briefly described the necessary computational steps required in order to estimate the signal intensities of VLF/ELF radiation. In our work, the entire process was modeled numerically using three computer codes:

(a) chemical model computer code,
(b) electron heating computer code,
(c) radiation computer code.

Other work, by STUBBE and KOPKA (1977), for instance, developed analytical expressions for the VLF/ELF radiation by assuming that temperature variations can be expressed as $e^{j\omega t}$. In the present approach numerical methods are employed in order to include self-absorption effects and temperature-dependent time constants.

The basic steps taken to calculate the ELF/VLF fields are as follows: from the 10.7 cm solar flux and solar X-ray data on a given day for the latitude and longitude of the heater site, the chemical model code creates the electron density distribution for the D- and lower E-regions (see ROWE *et al.*, 1974). The output from this code is used in the electron heating code (TOMKO, 1981), along with parameters of the heating facility such as frequency, polarization mode, radiated power, pulse width and repetition rate, to create a file of time history of electron temperature as a function of altitude. Also calculated are the values of σ_{xx}, σ_{yy}, and σ_{xy} vs time and altitude. From these values the horizontal currents are calculated on the basis of a dynamo electric field of 25 mV m^{-1} directed in the east–west direction. Finally the radiation code (RICHARDSON, 1982) calculates the expected total field at ground level. In this calculation the spatial volume of

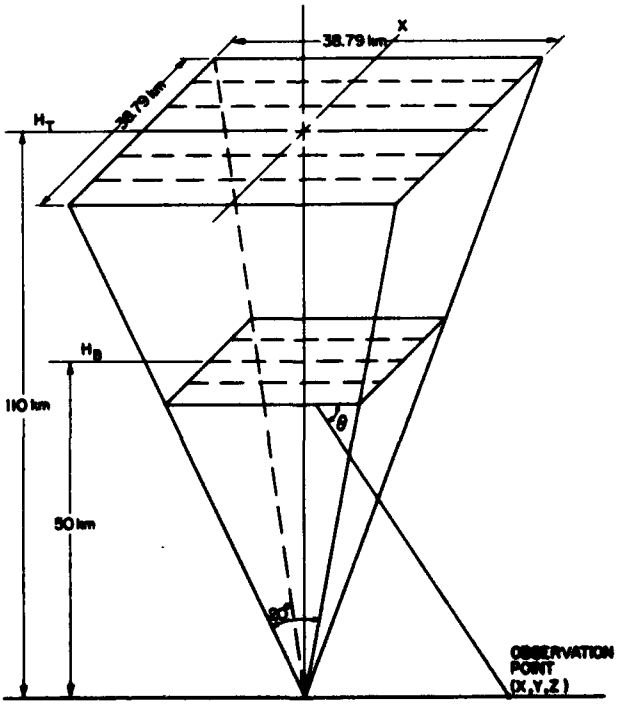

Fig. 3. Geometry of modified current region.

modulated current is assumed to be in free space. The free space field is multiplied by an absorption term for the pertinent VLF/ELF signal to approximate the actual field.

3. EQUIPMENT

3.1. *Description of VLF/ELF receiving facility*

A block diagram of the receiving system used for this work is shown in Fig. 4. The receiving system is a tuned ELF receiver employing synchronous detection. The in-phase and quadrature outputs of the synchronous detector, along with the A.G.C. voltage from the heater monitor receiver, are sampled by the data acquisition unit and recorded on magnetic disk. The A.G.C. voltage of the heater monitor receiver is recorded in order to define the heater on-off status.

A balanced loop antenna 1 m in diameter consisting of 200 turns of No. 14 wire and having a tuned Q of 64 at 2.5 kHz was used. A 0.5 m diameter one turn calibration loop was located coaxially at a distance of 0.5 m from the main loop. The current through the calibration loop was measured with the aid of a 50 ohm resistor placed in series with the loop. The calibration loop was used to generate a known field intensity for calibration of the receiving system.

A Princeton Applied Research model 113, low noise high input impedance (100 Mohms) differential input preamplifier was used in the system. The gain of this preamplifier is normally fixed at 40 dB with a 3 dB bandwidth of 1–10 kHz when measurements are made at 2.5 or 5 kHz. The second filter and amplifier in the system has a bandwidth of only $\pm 2\%\, f_c$, where f_c is the center frequency, and a rolloff rate of 115 dB per octave. The gain of this amplifier is adjustable from zero to 60 dB in order to compensate for variations in the received signal strength. A Princeton Applied Research model 5204 synchronous detector with the input sensitivity adjusted to 2.5 mV full scale was used. The reference channel input to the detector is derived from a frequency standard accurate to two parts in 10^9; this stability allows the accurate measurement of phase changes in the ionospheric signal and also allows integration times of up to 30 s to be used at the output of the synchronous detector. A time constant of 30 s, corresponding to a 3 dB bandwidth of 0.005 Hz, is normally used in data recording.

Prior to the July 1981 observations, the receiver was not accurately calibrated, but for the July and December 1981 data the receiver was carefully calibrated. Calibration of the receiver is based on the following relationships. JEAN *et al.* (1961) give the mutual impedance between two coaxial one turn loops as

$$Z_{12} = (2\pi r_2)\frac{j\mu\omega}{\pi k}\left(\frac{r_1}{r_2}\right)^{1/2} \times\left[\left(1-\frac{k^2}{2}\right)K(k)-E(k)\right], \qquad (13)$$

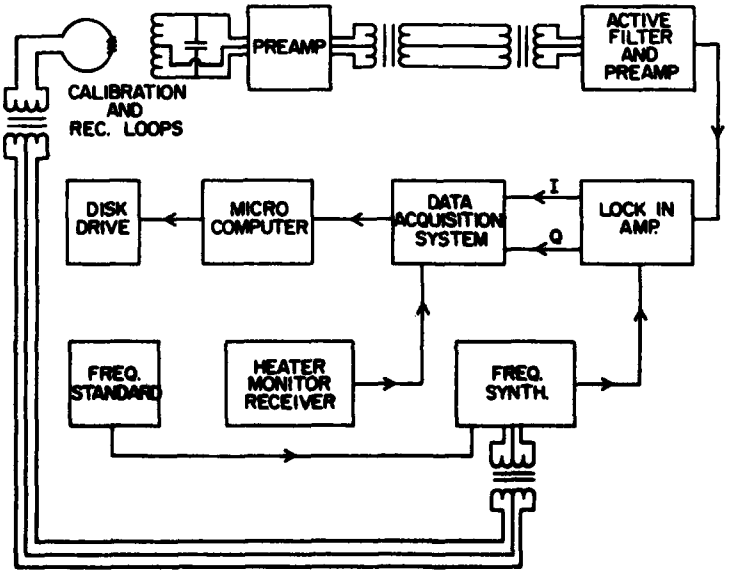

Fig. 4. Block diagram of the ELF/VLF receiving system.

where

$$k = \left[\frac{4r_1r_2}{(r_1+r_2)^2+d^2}\right]^{1/2},$$

r_1 and r_2 are the transmitting and receiving loop radius, respectively, d is the distance between loops, ω is the angular frequency of operation and $K(k)$ and $E(k)$ are elliptic integrals. The r.m.s. voltage V_2 produced across the receiver loop by a current I_1 in the calibration loop will then be

$$V_2 = I_1 Z_{12} NQ, \tag{14}$$

where N is the number of turns and Q is the tuned Q of the receiving loop. Using Faraday's law, the voltage which will appear across the receiving loop due to a traveling electromagnetic wave will be

$$V_{2T} = -jQ\omega BAN \cos\phi, \tag{15}$$

where ω is the angular frequency of the wave, B is the r.m.s. magnetic flux density (Wb m^{-2}), ϕ is the angle between B and the axis of the loop, and A is the effective area of the loop (m^2). Taking the magnitude of V_{2T}, assuming $\phi = 0$ and setting $V_2 = V_{2T}$, one obtains

$$|B| = \frac{|I_1|Z_{12}}{\omega A}. \tag{16}$$

Thus one obtains the relationship between the magnitude of the current in the calibration loop and the magnitude of a traveling electromagnetic wave which produces the same voltage across the receiving loop. Since $B = \mu H$ equation (16) becomes

$$|H| = \frac{|I_1|Z_{12}}{\omega A\mu}, \tag{17}$$

where $|H|$ is the equivalent magnetic field intensity (A m^{-1}). Upon substituting the proper constants into equations (13) and (15) one finds that for the antenna equation (17) reduces to

$$|H| = |I_1| \times 8.6 \times 10^{-2}. \tag{18}$$

The actual calibration of the system proceeds as follows: a large, approximately 1 V, signal is placed across the calibration loop and series resistor. The level of this signal is accurately measured and the current through the loop calculated. The calibration signal is then attenuated by 80 dB and the equivalent magnetic field intensity calculated from equation (18). A recording several minutes long is then made of the known calibration signal. This procedure is repeated for each frequency of operation and at calibration signal levels other than 80 dB below the 1 V reference level in order to check for any frequency dependence in the calibration or nonlinearity in the receiver.

During the analysis of ELF data the amplitude of the received data, with appropriate corrections for changes in receiver gain, is compared with the amplitude of the calibration recording in order to ascertain the field intensity of the ELF signal.

3.2. *Parameters of the heating facilities*

The facilities at Arecibo, Puerto Rico and Tromsø, Norway have been used to modulate the ionospheric current system. Most of the data presented in Section 4 of this paper were obtained at the Arecibo Observatory. A few long-path measurements made at University Park, Pennsylvania, relied upon the Tromsø facility. Table 1 summarizes the important parameters associated with each ionospheric heating facility.

4. OBSERVATIONAL RESULTS

4.1. *Measurements at the Arecibo Observatory*

VLF/ELF data were observed over four heating campaigns at the Arecibo facility. Measurements were made directly beneath the modified current region at daytime and nighttime. Table 2 summarizes important information about the campaigns, such as dates, HF heater parameters, and received signals. The last two columns of Table 2 give an indication of the solar and geomagnetic activity at times of VLF/ELF reception.

Table 1. Comparison of the Arecibo and Tromsø HF ionospheric heating facilities.

	Arecibo, Puerto Rico	Tromsø, Norway
Geographic location	18°N, 67°W	70°N, 19°E
Magnetic latitude	32°N	67°N
Magnetic dip	51°	78°
Frequency	3–12 MHz	2.75–8 MHz
Power	800 kW	1.2–1.4 MW
	4 × 8 array of orthogonal non-planar log-periodic dipole arrays	6 × 6 array of orthogonal fan dipoles
Antenna zenith gain	23–26 dBi	24 dBi
Antenna beamwidth	5°–10°	8.5°
Effective radiated power	160–320 MW	300–350 MW

Table 2. Summary of data and parameters for four campaigns at the Arecibo Observatory

Campaign	Dates	Heater frequency (MHz)	Heater power (MW ERP)	VLF/ELF frequencies (Hz)	Solar 10.7 cm flux (10^{-22} W m^{-2} Hz^{-1})	Range of hourly equatorial *Dst* values (gamma)
1	1–3 December 1980	3.175	75	4000, 5000	197.9–213.3	−16 to −40
2	24–30 March 1981	3.175, 8.175	150, 84	5000, 2500, 1000, 500	191.4–208.2	8 to −56
3	20–23 July 1981	3.170, 3.175	100, 125	Very weak signals, received sporadically	228.1–235.9	6 to −15
4	30 November–13 December 1981	3.170	75, 100	5000, 2500, 992.032, 574.712	230.3–292.4	6 to −23

The rest of this section will discuss in more detail the characteristics of the received VLF/ELF signal.

A typical data set contains in-phase and quadrature voltage signals recorded using the receiver system described earlier. These signals are then converted into amplitude and phase before being processed for possible indication of VLF/ELF signals. At the present, the data are processed using the fast Fourier transform algorithms of BERGLAND and DOLAN (1979). While the VLF/ELF waves are generated by pulsing the HF high power transmitter at a VLF/ELF rate, the transmitter is turned on and off periodically in order to facilitate further the detection of weak signals. The on-off periods are typically either 4 or 10 min in duration.

In applying FFT data processing, special care was exercised in optimally choosing the sample length in view of the extremely weak signals which were being received. If the sample length is limited to one on-off period, a momentary noise burst could lead to a false indication of the fundamental component. On the other hand, if it contains too many on-off periods, it could obscure the short-term presence of true ELF signals. Thus the data were processed with a sample length of three on-off periods for data taken with the 4 min period; a sample length of two on-off periods was used for data taken with a 10 min period.

Figure 5 shows a sample of processed data obtained by pulse-modulating the 3.170 MHz heater HF carrier at a frequency of 2.5 kHz with a 4 min on-off period; the heater was on for 2 min and then off for 2 min. Figures 5(a) and (b) show the amplitude and the phase of the signal respectively, whereas Fig. 5(c) shows the spectral components obtained by applying the FFT analysis to the amplitude of the signal. The times when the heater was on are indicated along the timebase of Figs 5(a) and (b), and commence at 2020, 2024 and 2028 UT. The 2.5 kHz amplitude clearly alternates between on and off periods indicating the presence of 2.5 kHz signals. It should also be noted that the phase signal is well locked at a nearly constant level during the heater-on period, while it is fluctuating randomly during the heater-off period due to absence of a signal. This feature demonstrates the capability of the measurement

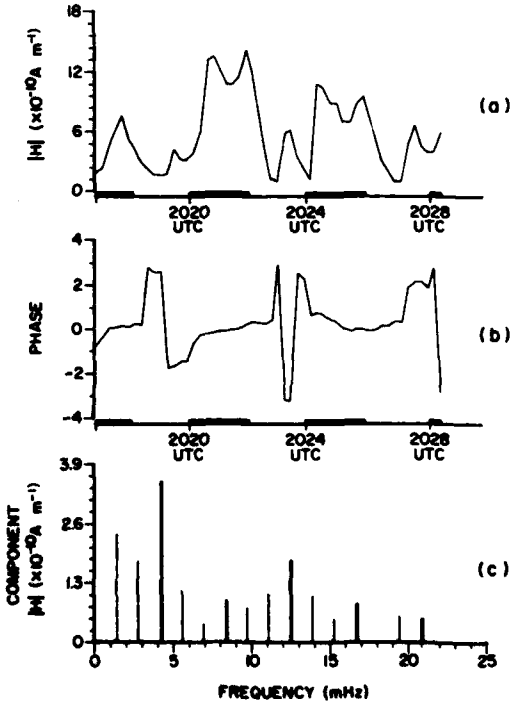

Fig. 5. Amplitude, phase (rad) and spectrum of amplitude fluctuations of 2.5 kHz signals measured at Arecibo from 2017 to 2028 UT on 3 December 1981.

technique to observe the phase variation of VLF/ELF signals.

Presence of a 2.5 kHz radiated signal is also evident from Fig. 5(c) where the fundamental frequency component of 4 min on-off period, 4.17 mHz, and its harmonic components, are shown with thicker lines. The fundamental frequency component is dominant; it is interesting to note that odd harmonic components prevail, a feature which is explained by the near-square-wave time functions. Additional data are shown later in Fig. 7, describing 'false' tests, in which the presence of a strong ELF signal at 2.5 kHz is also evident. Furthermore, it should be noted that these data shown in Fig. 7 were observed continuously over an hour near noon whereas the data shown in Fig. 5 were recorded during late afternoon.

4.2. *Long-path measurements*

In January 1981 an attempt was made to detect long-path ELF signals at the Pennsylvania State University, University Park, Pennsylvania. The origin of the ELF generation was Tromsø, Norway, where Dr Peter Stubbe of the Max-Planck-Institut für Aeronomie was investigating local ELF phenomena due to polar electrojet modulation. This effort took place, over five days, with 3–8 h of data each time. Since it was a first attempt at recording long-path signals, the measurements encompassed several different modes of operation: on-off mode at fixed ELF as described earlier in Section 4.1, on-off mode with ELF stepped periodically over three different frequencies, CW mode, etc.

Preliminary results obtained for an 8 h test on 11 January 1981, are presented in this section. The main objective of the measurements was to evaluate the feasibility of long-path detection of ELF waves, using an on-off mode with a 10 min period.

The FFT analysis shown in Fig. 6(a) depicts the time variation, throughout an 8 h period, of the strength of the fundamental frequency component, 1.67 mHz, of the 10 min on-off period. Figures 6(b) and (c) show the spectral distribution of two data samples taken at 2114 and 1932 UT, respectively. The fundamental components corresponding to these two samples are also identified in Fig. 6(a). Figures 6(b) and (c) show not only a distinct fundamental frequency component of 1.67 mHz but also strong odd harmonic components as were seen in Fig. 5(c). These two results are presented not only because they show distinct ELF signal components but also because the times at which they were taken are believed to coincide with enhanced polar electrojet activity seen at Tromsø.

Although at present only a portion of the long-path data have been processed the results obtained so far are encouraging.

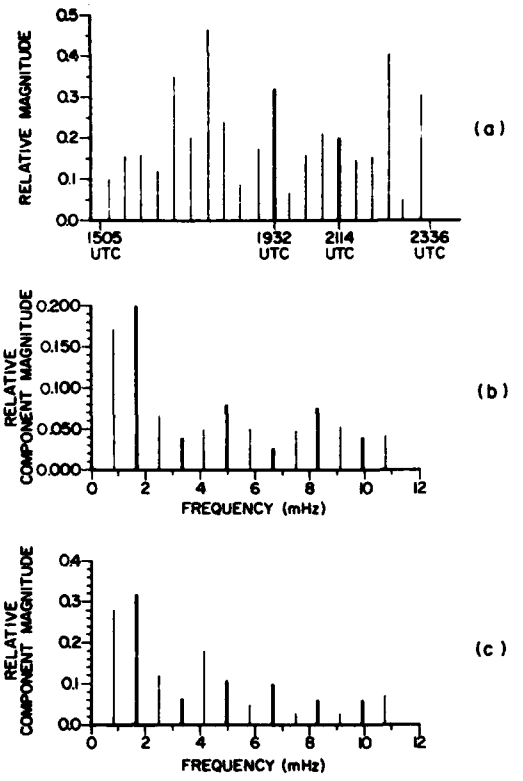

Fig. 6. Temporal variation of (a) amplitude of fundamental component and (b) and (c) spectrum of amplitude fluctuations demonstrating the on-off period for 2.073 kHz signals received from Tromsø during the period 1505–2336 UT on 11 January 1981.

4.3. *'False' test investigations*

Numerous possible sources of falsely generated signals have been investigated. Two of the most probable sources which were extensively studied are: (1) reception of ELF sidebands radiated by the heating transmitter and (2) nonlinear demodulation of the heating signal in the ELF receiver.

An example of the possible generation of false signals caused by the sidebands of the heating transmitter is seen by choosing the modulation frequency to be 2.5 kHz when the HF heater frequency is 3.170 MHz; in this case the heating transmitter could possibly produce a sideband at 2.5 kHz. Although the order ($n = 1267$) of this particular sideband is quite large, the heating transmitter is extremely powerful and the ELF receiver is very sensitive, allowing for the possible reception of radiated sidebands.

In order to test for this effect, the following

experiment was performed several times. The heating transmitter was operated at 3.170 MHz with 2.5 kHz square-wave modulation until a reasonably strong ELF signal was positively received as shown in Fig. 7(a). Then the frequency of the heating transmitter was changed to 3.171 MHz and the signal shown in Fig. 7(b) was observed. At this new heating frequency all possible sidebands produced by the heater are well outside the bandpass of the synchronous detector (0.005 Hz). Since Figs 7(a) and (b) show essentially no change in the strength of the received ELF signal for 3.170 and 3.171 MHz, it is concluded that no false effect due to the radiation of sidebands from the heating transmitter is contaminating the actual received signals.

A second source of false signals in the system could be nonlinear demodulation of the heating signal in the ELF receiver. In order to establish that the system is rather immune to this type of effect three steps were taken. First the threshold level of HF signal strength required at the input of the preamplifier to produce a detectable false effect was determined; second, the level of HF signal present at the input of the preamplifier during an actual experiment was measured and, third, filter traps at the heater frequency were installed into the system. The HF traps used were made removable so that the ELF signal could be observed both with and without the traps in place.

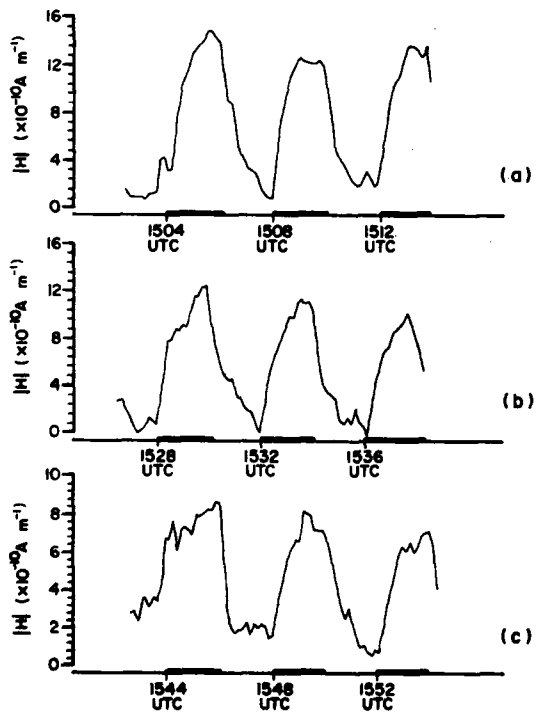

Fig. 7. Amplitudes of 2.5 kHz signals for studying false signal effects at Arecibo during the period 1500–1600 UT on 9 December 1981.

In order to determine the level of HF signal required at the preamplifier input to produce a false signal at the output of the detector, a balanced signal source at the heater frequency was injected into the input preamplifier of the ELF receiver with a 50% duty cycle and a pulse repetition frequency of 2.5 kHz; it was determined that 6.3 mV peak–peak or larger must be present at the input in order to produce a detectable false effect with the gain of the system set as for normal signal recording.

During the July 1981 observations the actual HF signal level at the input to the preamplifier was measured and found to be of the order of 1.0 mV peak–peak maximum. Thus the HF signal received by the loop antenna should not cause any significant nonlinear demodulation effects to occur in the ELF receiver.

Although the tests outlined above would reasonably preclude any nonlinear demodulation in the ELF receiver an additional test was made in which HF traps tuned to the heater frequency were connected across the inputs to the preamplifier. The traps which were used consisted of open circuited coaxial transmission lines one-quarter wavelength long at the heater operating frequency and produced a measured HF attenuation of 30 dB.

Figures 7(b) and (c) show the results of ELF signals received without and with the traps connected respectively. The small variation in the signal levels depicted in Figs 7(b) and (c) is due to a slow ionospheric fade and to a small change in the tuned characteristics of the receiving antenna after installation of the filters. Hence it is concluded that there was no significant demodulation of the transmitted HF signal by the ELF receiver.

5. DISCUSSION

This paper has shown that it is possible to detect the ELF/VLF radiation that results from modulating the dynamo current system by HF heating of the *D*- and lower *E*-layers of the ionosphere. Several campaigns of observations at the Arecibo Observatory have repeatedly shown that radiation from 500 to 5000 Hz can be received. This paper has examined the possibility of receiving falsely created signals, and concludes that the signals received are indeed generated within the ionosphere. A few long-path (Norway–Pennsylvania) propagation results have been described; here modulation of the polar electrojet was induced from Tromsø, Norway, during experiments being conducted by the Max-Planck-Institut für Aeronomie. The FFT

analyses indicate with reasonable certainty that the ELF radiation propagated over this long path. Considerable amounts of data were recorded during those experiments and are undergoing further analysis to evaluate the statistics associated with this successful detection.

The field strengths which were received cannot, unfortunately, be completely verified yet by the antenna model described in Section 2; this model predicts field strengths several times those that were actually measured. It is believed that predicting the modified currents from a change in conductivity is not accurate, and that the inductance of the current path may need to be included.

Acknowledgements—This work was supported by the Office of Naval Research, Contract N00014-81-K-0276. The Arecibo Observatory is operated by Cornell University under contract to the U.S. National Science Foundation. The long-path experiments were conducted in cooperation with Dr PETER STUBBE of the Max-Planck-Institut für Aeronomie. Solar geophysical data were provided during the Arecibo campaigns by the U.S.A.F. Solar Observatory at Ramey, Puerto Rico. Magnetometer data were supplied by the San Juan Observatory.

REFERENCES

BANKS P. M. and KOCKARTS G.	1973	*Aeronomy*. Academic Press, New York.
BUDILIN L. V., GETMANTSEV G. G., KAPUSTIN P. A., KOTIK D. S., MITYAKOV N. A., PETROVSKII A. A., RAPOPORT V. O., SAZONOV YU. A., SMIRNOV S. YU. and TRAKHTENGERTS V. YU.	1977	*Izv. vyssh. ucheb. Zaved.* **20**, 83.
GETMANTSEV G. G., ZUIKOV N. A., KOTIK D. S., MIRONENKO L. F., MITYAKOV N. A., RAPOPORT V. O., SAZONOV YU. A., TRAKHTENGERTS V. YU. and EIDMAN V. YA.	1974	*JETP Lett.* **20**, 229.
JEAN A. G., TAGGART H. E. and WAIT J. R.	1961	*J. Res.* **65C**, 189.
KAPUSTIN I. N., PERTSOVSKII R. A., VASILEV A. N., SMIRNOV V. S., RASPOPOV O. M., SOLOVEVA L. E., UGYACHENKO A. A., ARYKOV A. A. and GALAKHOVA N. V.	1977	*JETP Lett.* **25**, 228.
RISHBETH H. and GARRIOTT O. K.	1969	*Introduction to Ionospheric Physics*. Academic Press, New York.
ROWE J. N., MITRA A. P., FERRARO A. J. and LEE H. S.	1974	*J. atmos. terr. Phys.* **36**, 755.
STUBBE P. and KOPKA H.	1977	*J. geophys. Res.* **82**, 2319.
TURUNEN T., CANNON P. S. and RYCROFT M. J.	1980	*Nature* **286**, 375.

Reference is also made to the following unpublished material:

BERGLAND G. D. and DOLAN M. T.	1979	Programs for digital signal, processing. IEEE Press.
RICHARDSON C.	1982	Report PSU-IRL-MEMO-1, Ionosphere Research Laboratory, Pennsylvania State University, University Park, Pennsylvania.
STUBBE P.	1980	CCOG Handbook Circular Letter No. 2 (Edited by W. STOFFREGEN), Sweden.
TOMKO A. A.	1981	Report PSU-IRL-SCI-470, Ionosphere Research Laboratory, Pennsylvania State University, University Park, Pennsylvania.